The Tel Megiddo paleointensity project: toward a high resolution reference curve for archaeomagnetic dating

Ron Shaar[1*] Lisa Tauxe[2], Hagai Ron[1], Amotz Agnon[1], Yael Ebert[1], Israel Finkelstein[3]
[1] The Institute of Earth Sciences, The Hebrew University of Jerusalem, Jerusalem, 91904 Israel
[2] Scripps Institution of Oceanography, University of California San Diego, La Jolla, California 92093-0220 USA
[3] The Department of Archaeology and Ancient Near Eastern Civilizations, Tel Aviv University, Tel Aviv 6997801, Israel.

[*] Corresponding author
Ron Shaar, The Institute of Earth Sciences, The Hebrew University of Jerusalem, Jerusalem 91904, Email: ron.shaar@mail.huji.ac.il. Phone: 972-2-6584248

1. Introduction

It has been known for at least a century that the intensity of Earth's magnetic field is not constant over archaeological time scales, but instead, varies with time. Yet, the accepted working paradigm regarding the past several millennia has been that the intensity of the field ranged from about half to about 1.5 times the present field and that measurable changes in field intensity occur on periods of few centuries (Yang et al., 2000, Tauxe and Yamazaki, 2007; Genevey et al., 2008). However, it has been only recently recognized that changes in field intensity (*paleointensity*, for short) can be faster and stronger than previously assumed (Ben-Yosef et al., 2009; Shaar et al., 2011, 2015). The most dramatic illustration of paleointensity variations is "geomagnetic spikes", short sub-centennial episodes of extreme high field values. Geomagnetic spikes ca. 1000 BCE were recovered from Iron Age slag deposits in Timna and Faynan (Ben-Yosef et al., 2009; Shaar et al., 2011), and they possibly mark the climax of a longer period with unusually high field anomaly in the Levant.

Given a new working hypothesis stating the paleointensity variations can be large and fast, we have started some years ago a multi-institutional project aimed at reconstructing paleointensity variations in the Levant from archaeological resources. This inter-disciplinary multi-institutional project gathers archaeologists and geophysicists from several institutes, including Tel-Aviv University, The Hebrew University of Jerusalem, Scripps Institution of oceanography, and the University of California San-Diego, among others. The project is designed to deliver in the long run a comprehensive high resolution paleointensity dataset that can be used for both geophysical exploration of the origin of Earth's magnetic field (geodynamo), and archaeomagnetic dating.

Tel Megiddo is the first tell in Israel to be investigated systematically for paleointensity. To date, this effort includes analyses of forteen strata from the Bronze to Iron Age. We report here the results of the first phase of this on-going project. An accompanying article discussing the geophysical implications of the study is published elsewhere (Shaar et al., 2015b).

The explicit objectives of the project at Tel Megiddo are twofold. First, we aim at utilizing the precise high resolution chrono-stratigraphy of Tel Megiddo in order to obtain precise high resolution paleointensity record of the Bronze and Iron Age. Second, we aim at

standardizing the paleointensity procedure throughout all stages of research, from selecting the samples, preparing them for measurements, laboratory protocols, and finally data analyses. By establishing a standard working routine we seek to put a robust methodological platform for a long-term large scale research.

2. Methods

2.1. Samples

We collected 66 pottery vessels from 11 strata (J-4, J-6, F-13, F-10, K-8, K-6, H-9, H-7, H-5,H-3) and five cooking ovens (tabuns) from four strata (K-9, H-12, Q-4, Q-5). These baked clay objects are capable of recording a magnetic signal on cooling, and retaining a *Thermomagnetic Remanent Magnetization (TRM)* from which paleointensity information can be retrieved (see below). From each stratum we collected at least four vessels. When possible, we preferred thin, well sorted fine-grained, thoroughly burnt pottery sherds from whole, or restored vessels. Preference was given to domestic cheap vessels as it is more likely that these vessels were manufactured near the site, and best fit the chronological context of the archaeological stratum from which they were found. The pottery samples were collected from storehouses located at the Institute of the Archaeology, Tel Aviv University, and from the Israel Antiquities Authority.

Samples were prepared by breaking each potsherd (i.e. *sample*) into 4-10 smaller fragments (i.e. *specimens*). Each specimen was wrapped in glass filter paper and glued inside a glass vial, 12mm in diameter, using Potassium Silicate (KASIL) glue. Measurements were carried out at the paleomagnetic laboratory of Scripps Institution of Oceanography (SIO), University of California San Diego, using laboratory built paleointensity ovens, and at the paleomagnetic laboratory of the Institute of Earth Sciences, the Hebrew University of Jerusalem (HUJI), using a modified ASC TD-48 oven (Shaar et al., 2010).

2.2. Brief outline on the paleointensity method

The basic assumption underlying the Thellier-Thellier paleointensity method (Thellier and Thellier, 1959) is that TRM (magnetization acquired on cooling) is quasi-linearly proportional to the intensity of the field (B) in which it was acquired:

$$(TRM = \alpha B). \quad \text{Equation 1}$$

The laboratory procedure in the Coe variant of the Thellier method (Coe et al., 1967) is illustrated in Figure 1. The procedure involves a series of double heating steps at progressively elevated temperatures through which the ancient TRM (TRM_{anc}) is gradually replaced by a laboratory TRM (TRM_{lab}) acquired in a controlled field (B_{lab}). The measurements through this procedure are plotted on a so-called “Arai plot” (Nagata et al., 1963) displaying the ancient TRM (gradually erased) on the y-axis and the laboratory partial TRM (pTRM) (gradually acquired) on the x-axis (Figure 1). First, the natural remanent magnetization (NRM) of the specimen (assumed to be thermal in origin) is measured and plotted on the intercept of the y-axis of the Arai plot (Figure 1a). Then, the specimen is heated to temperature T_1 under a null magnetic field (“zerofield”). This procedure demagnetizes part of the ancient TRM (Figure 1b). The specimen is then heated again to T_1, but cooled in the presence of controlled field B_{lab} (“infield”) leading to an acquisition of laboratory pTRM. Using vector arithmetic, the portions of $TRM_{ancient}$ “remaining” and $pTRM_{laboratory}$ “acquired” are calculated and the point T_1 (pTRM remaining versus pTRM acquired) is plotted on the Arai plot (Figure 1b-c). These double heating steps continue at

increasingly elevated temperatures, where at every second step we run an "alteration check" (Coe et al., 1978), by which we repeat an "infield" step at a lower temperature (triangles in Figure 1d). This step tests whether alteration of the ferromagnetic minerals had occurred by heating the sample. Finally, after completing all the steps (usually 10-15 different temperatures are required), the nature of the Arai plot can determine whether a paleointensity can be calculated. If the plot conforms an ideal straight line, as shown in Figure 1e, then from the slope of the line (equal to $TRM_{ancient}/TRM_{laboratory}$), the paleointensity is calculated by:

$$B_{ancient} = slope \cdot B_{laboratory} \qquad \text{Equation 2}$$

In this study we follow the IZZI variant of the Thellier method (Tauxe and Staudigel, 2004), by which the order of the "infield" and the "zerofield" alternate in each succeeding step. Also, we carry out two additional experiments for calculating a correction for TRM anisotropy (e.g. Selkin et al., 2000) and for the effect of cooling rate (e.g. Genevey and Gallet, 2002). The anisotropy correction compensates for the dependency of TRM on the magnetic fabric (as the direction of B_{lab} is different than B_{anc}). The cooling rate correction compensates for the dependency of TRM on cooling rate (the ancient cooling time was many hours, while in the lab cooling takes place only 20-40 minutes).

A complete paleointensity procedure is a process requiring 30 to 50 heating steps, each takes 1-2 hours (for a batch of 54-72 specimens). This time, combined with the time required to measure the specimens makes the Thellier-Thellier method laborious and time consuming. The time and the effort built into the laboratory protocol is perhaps the main weakness of the method.

2.3. Standardizing data analyses procedure

One of the most difficult paleointensity methodological problems to deal with concerns data analysis. Here, in addition to the Arai plot, we use 'Zijderveld' plots (Zijderveld, 1967) of Cartesian components (x,y,z) of the zero field steps, plotted as x versus y and x versus z as in the insets to Figure 2. The root of the data analysis problem is that often specimens do not yield ideal straight lines in both the Arai and the Zijderveld plots as in Figure 2a. Instead, there may be a linear or quasi-linear segments that could be interpreted differently by different researchers. The problem of ambiguity in the interpretation inserts considerable noise to the published paleointensity database. To address this problem Shaar and Tauxe (2013) developed a computer program for automatic interpretation. This program is capable of analyzing many thousands of specimens (the long term target of the project) in a consistent, objective, and reproducible fashion, while calculating robust error estimations of the results. For more details see Shaar and Tauxe (2013) and Shaar et al. (2015a). To make the automatic interpretation meaningful, the user has to choose specific criteria for screening out only the most "reliable" results (e.g. Figure 2a or similar). This is done by a set of statistics defined in Shaar and Tauxe (2013) and Paterson et al (2014). Figures 2b-d shows some examples of specimens failing the criteria used in this study. Figure 2b shows an Arai plot with only partial linear segment; Figure 2c shows a zigzagged non-linear pattern; Figure 3d shows non-linear Zijderveld plots in the inset (see Paterson et al., 2014 for definitions).

A discussion of the various paleointensity statistics and the acceptance criteria is beyond the scope of this article. Yet, for the sake of completeness we list in Table 1 the criteria used in this study. For more details see Paterson et al (2014) and Shaar et al (2015b).

3. Results

In total we analyzed 388 specimens collected from 66 pottery samples and 5 ovens. Of these, 297 specimens and 39 samples passed our selection criteria, which are significantly stricter than what is commonly sued in paleointensity studies. This yields success rates of 77% at the specimen level and 60% at the sample level. Table 2 lists sample level paleointensity (average of at least 3 specimens). Figure 3 plots sample means versus age where pottery data are shown in red and ovens are shown in green. There is an agreement between data obtained from pottery and ovens supporting the reliability of the procedures and the materials.

We note some interesting features in the data shown in Figure 3. The field intensity before ca. 1800 BCE was 30-50 μT, that is, of the order of today's field (45 μT at Megiddo). After a local minimum at the 18th century, the field gradually increased, and from the 13th century onward the field reached very high values of between 50-95 μT (Figure 3b). The climax of this high field episode has a double peak shape: a local maximum at ca. 1000 BCE (stratum H-9), a local minimum during the 9th century (stratum H-7) and a second maximum at ca. 735 BCE (just before the destruction layer H-3). The two peaks at H-9 and H-3 are characterized with a large scatter of the data suggesting that the field changed rapidly during the time interval represented by the layers.

4. Discussion

Toward a master Levantine Archaeomagnetic Compilation (LAC)

One essential contribution of the Tel Megiddo paleointensity project is delivering some useful methodological improvements. To emphasize these improvements, we show in Figure 4 all published paleointensity data from the Levant. The picture from the entire legacy data is complicated, noisy, and shows some significant discrepancies. This is not surprising considering the variability of the legacy data in experimental methods, laboratory protocols, interpretation and error estimation approaches, selection criteria, averaging schemes, and assessment of anisotropy and cooling rate corrections. In addition, some legacy data employed different and sometime contradicting and irreproducible dating methodologies and, in cases, outdated chronologies.

We recall that our long-term goal is to provide a consistent and coherent paleointensity curve for archaeomagnetic dating and geodynamo research. Hence, in an effort to minimize paleointensity uncertainties in Figure 4 we adopt the automatic interpretation technique (Shaar and Tauxe, 2013) and construct a new compilation namely "Levantine Archaeomagnetic Compilation" (LAC). To minimize dating uncertainties we apply in the LAC an "Age Quality" index following Ben-Yosef et al., 2008ab, whereby only "grade 1" ("Excellent dating quality") are included. The combined dataset from all the studies published by our research group (Ben-Yosef et al., 2008ab, 2009; Shaar et al., 2011, 2015a,b) is analyzed using the criteria in Table 1, and displayed in Figure 5 in color symbols. As the local intensities are dependent of the site latitude the field values (measured in tesla) are converted to Virtual Axial Dipole Moments (VADMs, see Tauxe et al., 2010) – the strength of a hypothetical bar magnet centered in the Earth (given in units of magnetic moment, Am^2) and aligned with the spin axis that would give rise to the geomagnetic field intensity observed at the site latitude. For comparison, we also plot in open black symbols the data from Syria (Genevey et al., 2003; Gallet et al., 2005, 2006, 2008,2014, 2015; Gallet and Butterlin, 2015; Stillinger et al., 2015). These Syrian data were published without the

measurement data and cannot be re-interpreted using our criteria and automatic procedure. The main reasons for not including in Figure 5 all the published datasets shown in Figure 4 are problematic correlation between the Mesopotamian, Israeli, and the Egyptian chronologies, and insufficient (or problematic) experimental and chronological information.

Figure 5 displays a coherent and consistent picture of the geomagnetic field behavior in the first three millennia BCE, where the Mesopotamian and the Israeli datasets show excellent agreement in periods where they overlap, and mutually complement each other in others. During the first half of the 3rd millennium BCE the field was relatively low; in the second half of the 3rd millennium BCE the field reached VADM values of up to 110 ZAm^2 and then gradually decreased to a local minimum at ca. 1800 BCE. From ca. 1800 BCE the field intensity increased until the double-peaked maximum shown in Figure 5b.

Looking at Figure 5, one may ask why the LAC data points (colored symbols) are not exactly the same values as those published in our previous articles (Ben-Yosef et al., 2008a,b; 2009; Shaar et al., 2011). This issue is most apparent in the Iron Age (Figure 5b) and is the direct result of our new standardized interpretation protocol in which we prefer the automatic (objective) procedure over of the previous manual (subjective) interpretation approach. Also, we treat all samples identically, thus comparing "apples with apples", and apply selection criteria (Table 1) that are much stricter then we used in our previous publications. We underline the point that the LAC depends on the acceptance criteria, and if one chooses to use different criteria than the ones listed in Table 1, the paleointensity estimations, and the resulting LAC paleointensity curve will be slightly different.

5. Summary

- Tel Megiddo is the first tell in Israel to be systematically analyzed for paleointensity. This is our first attempt to use well-dated multi-strata site for constructing a regional paleointenisty variation curve.
- We report 39 new paleointensity estimations covering the Bronze and the Iron Age.
- The new data from Tel Megiddo is consistent with contemporaneous data obtained from pottery (Tel Hazor) and slag (Timna, Feynan, and Cyprus). Tel Megiddo also shows excellent agreement with paleointensity data derived from Mesopotamian sites in Syria.
- The overall paleointensity data from the Levant, with the significant contribution of Megiddo illustrate only moderate scale variations in field intensity during the third and the second millennia BCE. Yet, after a local minimum at ca. 1800 BCE with values similar to today's field, the field showed a fast increase until an exceptionally high double-peaked maximum spanning between the 10th and the 8th centuries BCE. The high field period was accompanied by at least two geomagnetic spikes: one at ca. 980 BCE (Ben-Yosef et al., 2009; Shaar et al., 2011), and another at the beginning of the 8th century BCE (new data from H-3 destruction layer).
- One of the main future challenges in Levantine archeaomagnetism is using the method described here for producing much more high resolution data that can be

used in the long-run as a robust master curve for archaeomagnetic paleointensity dating.

Acknowledgements

We thank Eran Arie, Mario Martin, Norma Franklin, and Yaniv Agmon from Tel-Megiddo expedition for their help in collecting the samples. Partial funding for this research was provided by Israel Science Foundation Grant No. 1181/12 to AA, and National Science foundation grant EAR1345003 to LT.

References

Ben-Yosef, E., Ron, H., Tauxe, L., Agnon, A., Genevey, A., Levy, T. E., Avner, U. & Najjar, M. 2008. Application of copper slag in geomagnetic archaeointensity research. *Journal of Geophysical Research-Solid Earth,* 113.

Ben-Yosef, E., Tauxe, L., Levy, T. E., Shaar, R., Ron, H. & Najjar, M. 2009. Geomagnetic intensity spike recorded in high resolution slag deposit in Southern Jordan. *Earth and Planetary Science Letters,* 287**,** 529-539.

Ben-Yosef, E., Tauxe, L., Ron, H., Agnon, A., Avner, U., Najjar, M. & Levy, T. E. 2008. A new approach for geomagnetic archaeointensity research: insights on ancient metallurgy in the Southern Levant. *Journal of Archaeological Science,* 35**,** 2863-2879.

Chauvin, A., Garcia, Y., Lanos, P. & Laubenheimer, F. 2000. Paleointensity of the geomagnetic field recovered on archaeomagnetic sites from France. *Physics of the Earth and Planetary Interiors,* 120**,** 111-136.

Coe, R., Gromme, S. & Mankinen, E. 1978. Geomagnetic paleointensities from radiocarbon-dated lava flows on hawaii and question of pacific nondipole low. *Journal of Geophysical Research***,** 1740-1756.

Coe, R. S. 1967. Paleo-intensities of earths magnetic field determined from Tertiary and Quaternary rocks. *Journal of Geophysical Research,* 72**,** 3247-&.

Fisher, R. A. 1953. Dispersion on a sphere. *Proc. Roy. Soc. Lond,* 217**,** 295–305.

Gallet, Y. & Butterlin, P. 2015. Archaeological and Geomagnetic Implications of New Archaeomagnetic Intensity Data from the Early Bronze High Terrace "Massif Rouge' at Mari (Tell Hariri, Syria). *Archaeometry,* 57**,** 263-276.

Gallet, Y., D'andrea, M., Genevey, A., Pinnock, F., Le Goff, M. & Matthiae, P. 2014. Archaeomagnetism at Ebla (Tell Mardikh, Syria). New data on geomagnetic field intensity variations in the Near East during the Bronze Age. *Journal of Archaeological Science,* 42**,** 295-304.

Gallet, Y., Genevey, A. & Fluteau, F. 2005. Does Earth's magnetic field secular variation control centennial climate change? *Earth and Planetary Science Letters,* 236**,** 339-347.

Gallet, Y., Genevey, A., Le Goff, M., Fluteau, F. & Ali Eshraghi, S. 2006. Possible impact of the Earth's magnetic field on the history of ancient civilizations. *Earth and Planetary Science Letters,* 246**,** 17-26.

Gallet, Y., Le Goff, M., Genevey, A., Margueron, J. & Matthiae, P. 2008. Geomagnetic field intensity behavior in the Middle East between similar to 3000 BC and similar to 1500 BC. *Geophysical Research Letters,* 35.

Gallet, Y., Montana, M. M., Genevey, A., Garcia, X. C., Thebault, E., Bach, A. G., Le Goff, M., Robert, B. & Nachasova, I. 2015. New Late Neolithic (c. 7000-5000 BC) archeointensity data from Syria. Reconstructing 9000 years of archeomagnetic field intensity variations in the Middle East. *Physics of the Earth and Planetary Interiors,* 238**,** 89-103.

Genevey, A. & Gallet, Y. 2002. Intensity of the geomagnetic field in western Europe over the past 2000 years: New data from ancient French pottery. *Journal of Geophysical Research-Solid Earth***,** -.

Genevey, A., Gallet, Y., Constable, C. G., Korte, M. & Hulot, G. 2008. ArcheoInt: An upgraded compilation of geomagnetic field intensity data for the past ten millennia and its application to the recovery of the past dipole moment. *Geochemistry Geophysics Geosystems,* 9**,** 23.

Genevey, A. S., Gallet, Y. & Margueron, J. C. 2003. Eight thousand years of geomagnetic field intensity variations in the eastern Mediterranean. *Journal of Geophysical Research-Solid Earth,* 108.

Kirschvink, J. 1980. The least-squares line and plane and the analysis of paleomagnetic data. *Geophysical Journal of the Royal Astronomical Society***,** 699-718.

Nagata, T., Arai, Y. & Momose, K. 1963. Secular variation of the geomagnetic total force during the last 5000 years. *Journal of Geophysical Research,* 68**,** 5277-5282.

Paterson, G. A., Tauxe, L., Biggin, A. J., Shaar, R. & Jonestrask, L. C. 2014. On improving the selection of Thellier-type paleointensity data. *Geochemistry Geophysics Geosystems,* 15**,** 1180-1192.

Selkin, P. A., Gee, J. S., Tauxe, L., Meurer, W. P., Newell, A. J. 2000. The effect of remanence anisotropy on paleointensity estimates: a case study from the Archean Stillwater Complex. *Earth and Planetary Science Letters*, *183*(3), 403-416.

Selkin, P. A. & Tauxe, L. 2000. Long-term variations in palaeointensity. *Philosophical Transactions of the Royal Society of London Series a-Mathematical Physical and Engineering Sciences,* 358**,** 1065-1088.

Shaar, R., Ben-Yosef, E., Ron, H., Tauxe, L., Agnon, A. & Kessel, R. 2011. Geomagnetic field intensity: How high can it get? How fast can it change? Constraints from Iron Age copper slag. *Earth and Planetary Science Letters,* 301**,** 297-306.

Shaar, R., Ron, H., Tauxe, L., Kessel, R., Agnon, A., Ben-Yosef, E. & Feinberg, J. M. 2010. Testing the accuracy of absolute intensity estimates of the ancient geomagnetic field using copper slag material. *Earth and Planetary Science Letters,* 290**,** 201-213.

Shaar, R. & Tauxe, L. 2013. Thellier GUI: An integrated tool for analyzing paleointensity data from Thellier-type experiments. *Geochemistry Geophysics Geosystems,* 14**,** 677-692.

Shaar, R., Tauxe, L., Ben-Yosef, E., Kassianidou, V., Lorentzen, B., Feinberg, J. M. & Levy, T. E. 2015. Decadal-scale variations in geomagnetic field intensity from ancient Cypriot slag mounds. *Geochemistry Geophysics Geosystems,* 16**,** 195-214.

Shaar, R., Tauxe, L., Ron, H., Agnon, A., Ebert, Y., Zuckerman, S. & Finkelstein, I. 2015. Large geomagnetic field anomalies revealed in Bronze to Iron Age archaeomagnetic data from Tel Megiddo and Tel Hazor, Israel. *Earth and Planetary Science Letters,* under review.

Stillinger, M. D., Feinberg, J. M. & Frahm, E. 2015. Refining the archaeomagnetic dating curve for the Near East: new intensity data from Bronze Age ceramics at Tell Mozan, Syria. *Journal of Archaeological Science,* 53**,** 345-355.

Tauxe, L. 2010. *Essentials of Paleomagnetism,* Berkeley, University of California Press.

Tauxe, L. & Staudigel, H. 2004. Strength of the geomagnetic field in the Cretaceous Normal Superchron: New data from submarine basaltic glass of the Troodos Ophiolite. *Geochemistry Geophysics Geosystems***,** -.

Tauxe, L. & Yamazaki, T. 2007. Paleointensities. *Treatise on Geophysics* Elsevier.

Thellier, E. & Thellier, O. 1959. Sur l'intensiť e du champ magń etique terrestre dans le pasś e historique et ǵ eologique. *Ann. Geophys.,* 15**,** 285–376.

Yang, S., Odah, H. & Shaw, J. 2000. Variations in the geomagnetic dipole moment over the last 12 000 years. *Geophysical Journal International,* 140**,** 158-162.

Zijderveld, J. D. A. 1967. AC demagnetization of rocks: analysis of results. *Methods in paleomagnetism*, *3*, 254.

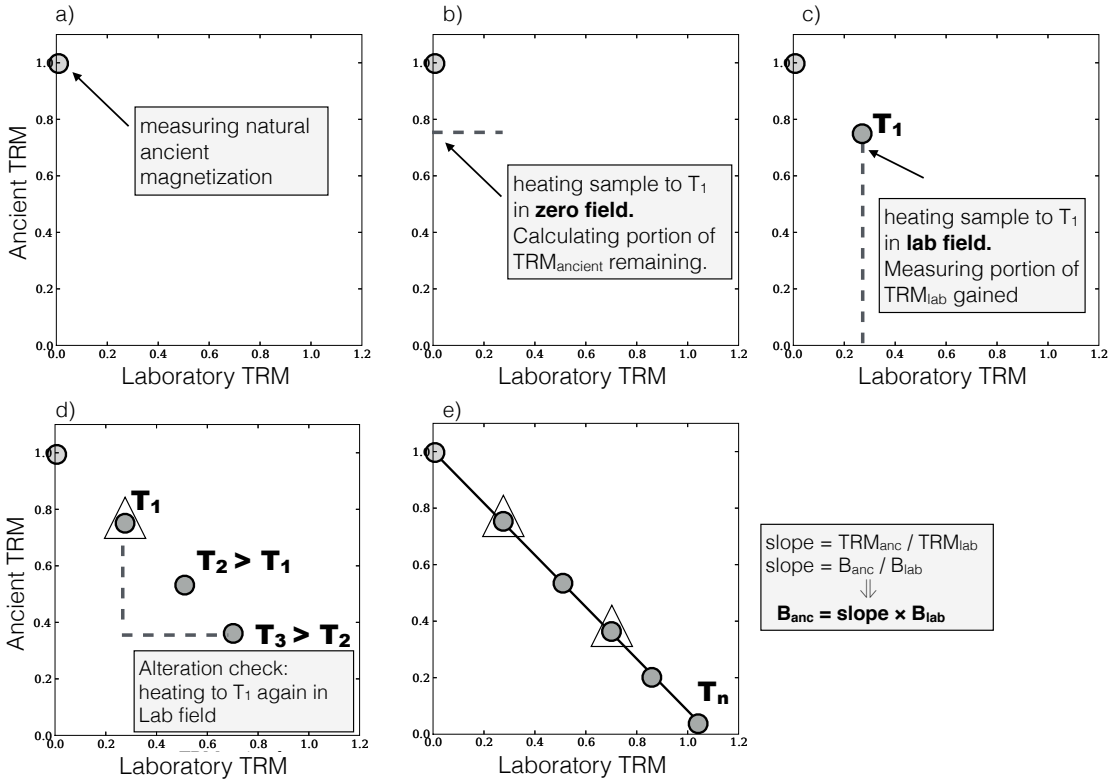

Figure 1: Schematic illustration of the Coe variant of the Thellier method (see text for details).

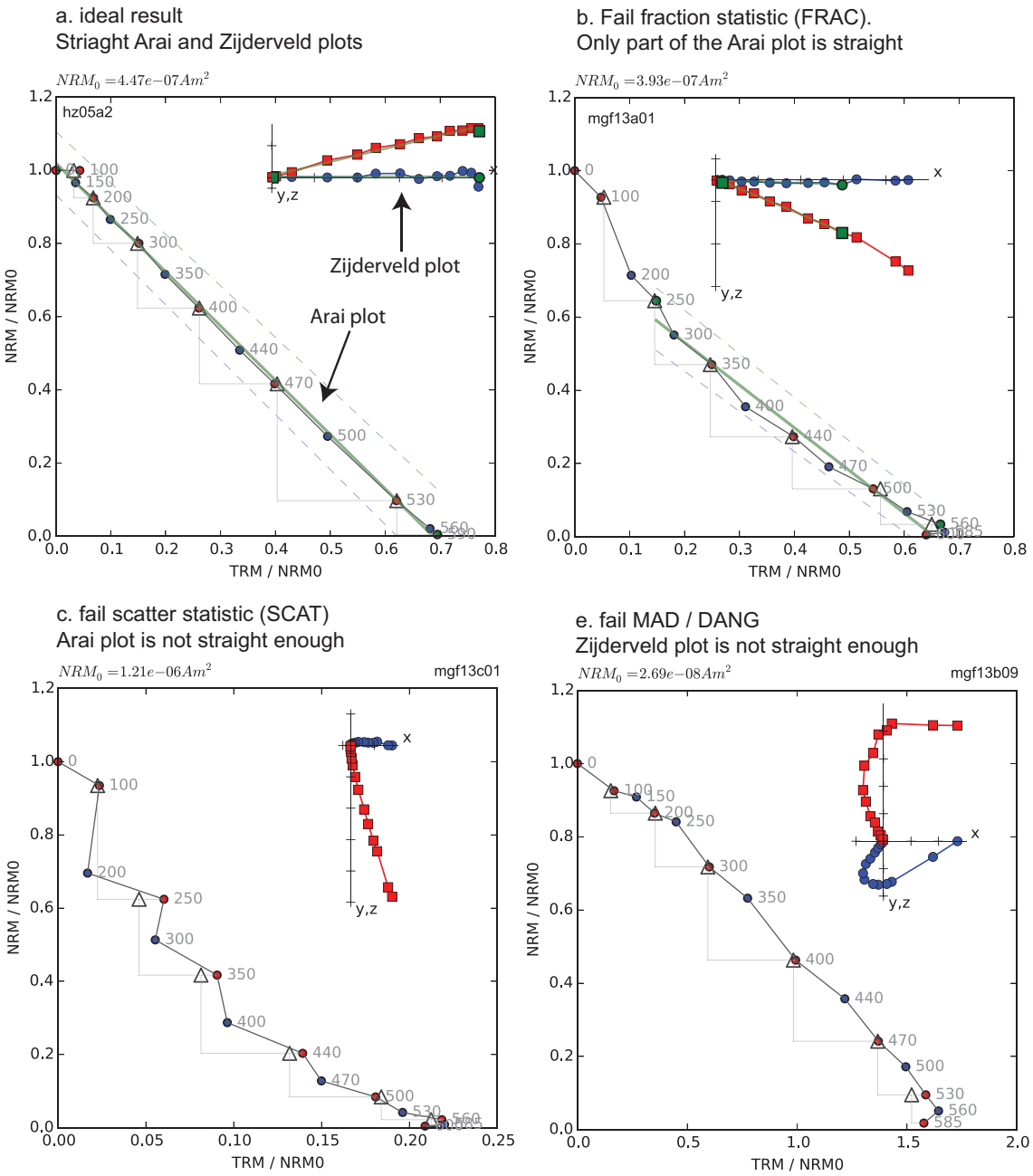

Figure 2: Representative result showing Arai plots (see text) and orthogonal Zijderveld plots (insets) of different pottery fragments. a) Ideal Arai and Zijderveld plots showing straight line. Paleointensity can be calculated without ambiguity from the slope of the Arai plot. b-d) Examples of results that were rejected by our strict acceptance criteria: b) Arai plot is only partly linear; d) A scattered non-linear Arai plot; d) Non-linear Zijderveld plots.

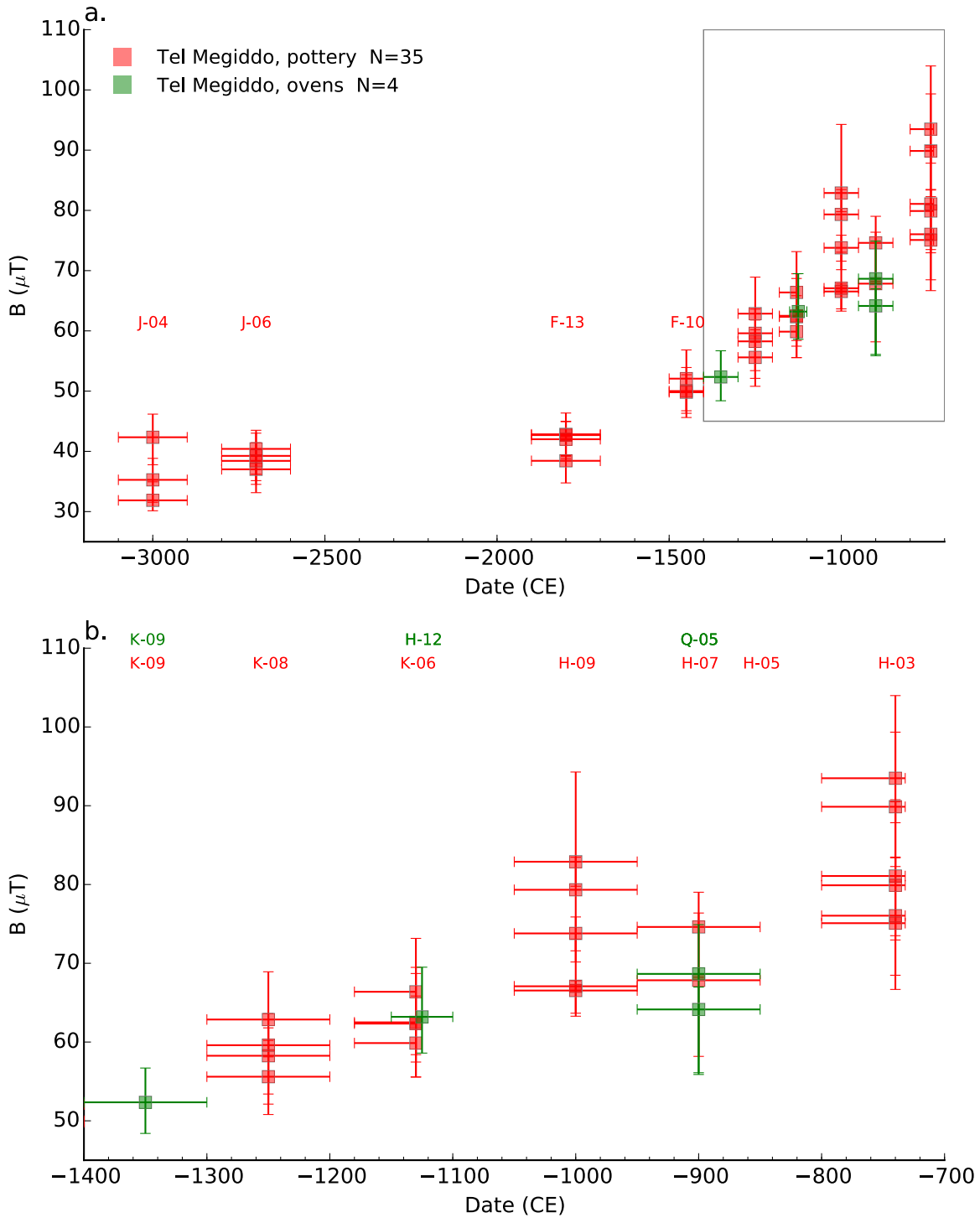

Figure 3: Paleointensity results from Tel Megiddo. Red (green) error bars denote for pottery vessels (Tabuns). Redrawn from Shaar et al. (2015b). (b) is the magnification of the rectangle in (a).

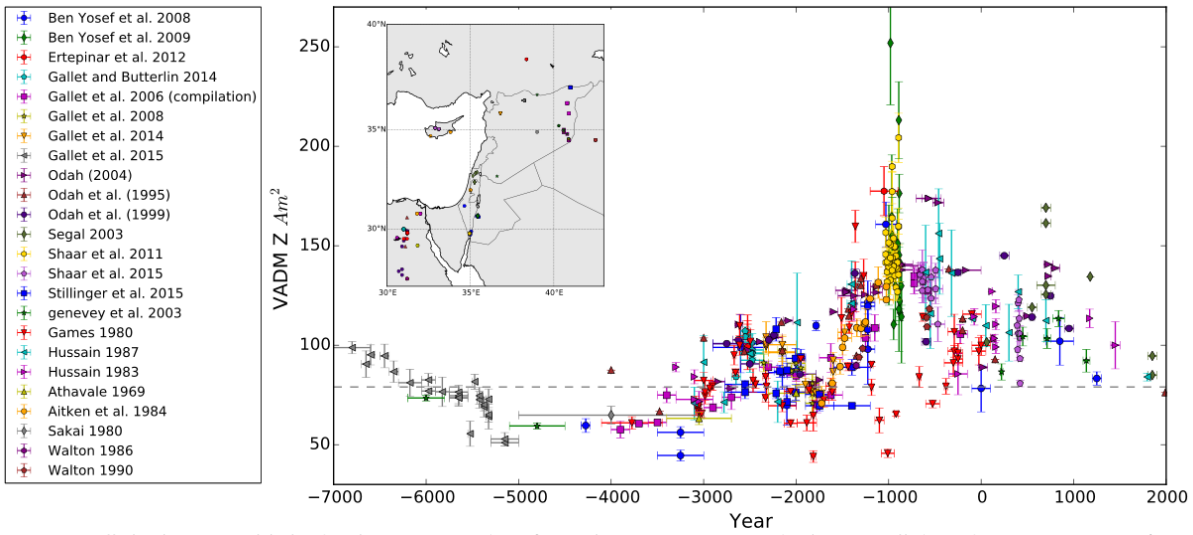

Figure 4: All the legacy published paleointensity data from the Levant unsorted. The overall data demonstrate significant discrepancies compared to the new compilation shown in Figure 5.

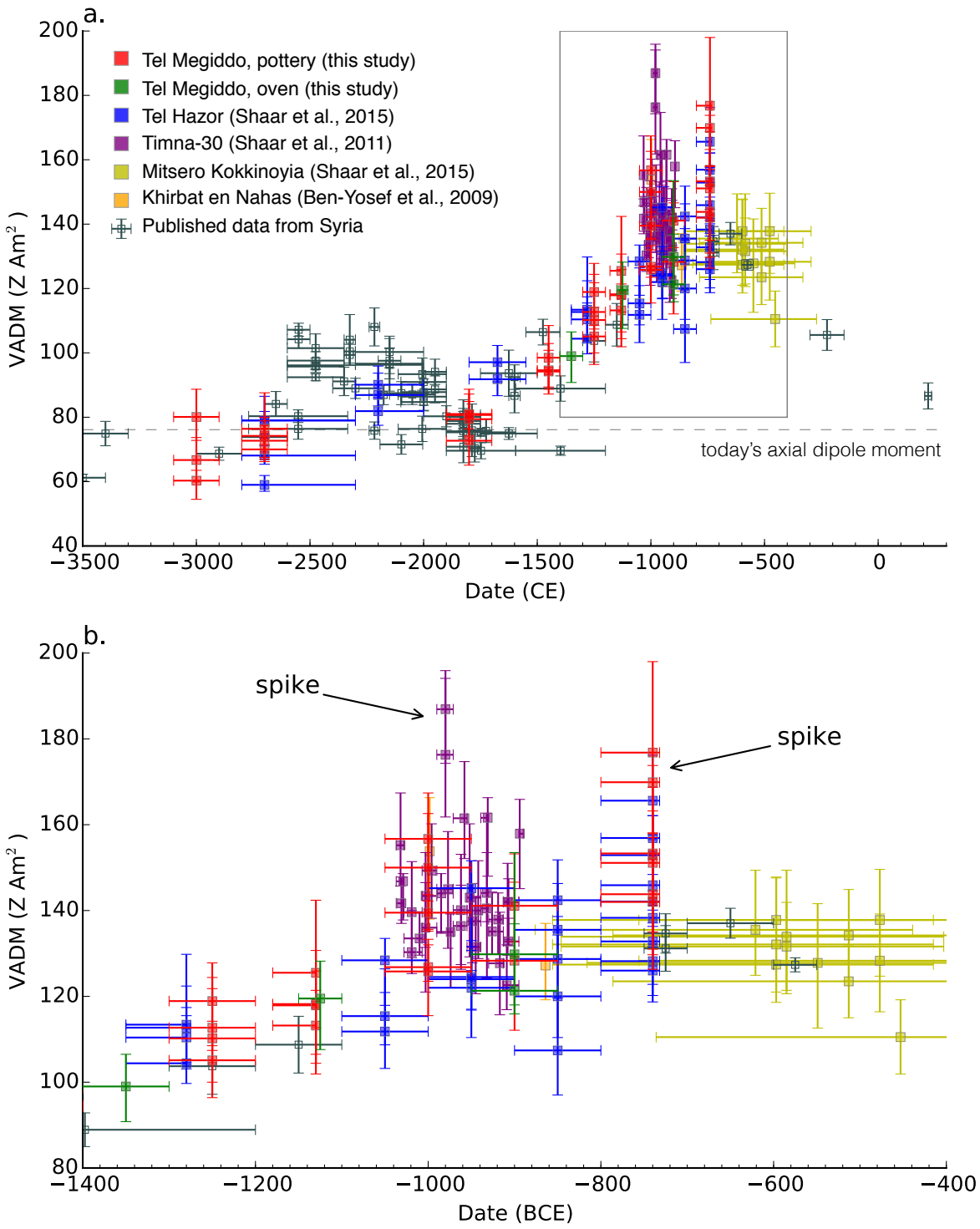

Figure 5: A new compilation of the Levantine paleointensity data (only the sites shown in Figure 6). Colored symbols denote for data interpreted for this study using the automatic interpretation technique of Shaar and Tauxe (2013) and the criteria listed in Table 1. Black open symbols are published results from Syria. Local intensity data (latitude dependent) are transformed to Virtual Axial Dipole Moment (VADM)–the geomagnetic dipole moment that would give rise to the observed intensity at the given latitude. The picture shows significant improvement from the Legacy data shown in Figure 4.

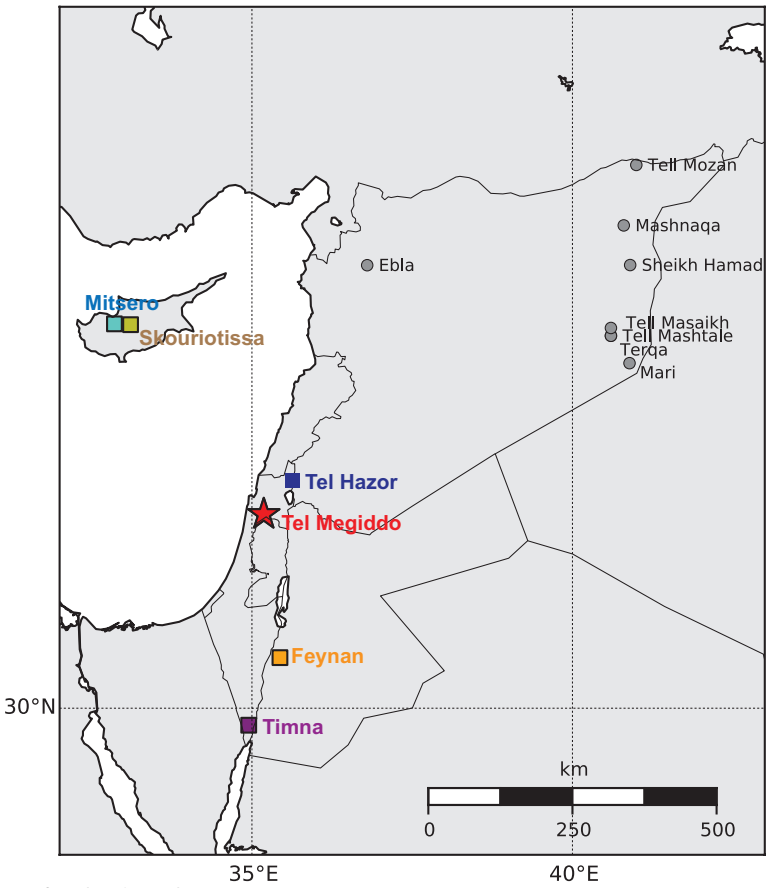

Figure 6: Location map for the data shown in Figure 5.

Table 1: Acceptance criteria

Criteria group	Statistic	Threshold value	Description	Reference[b]
Specimen paleointensity[a]	FRAC	0.79	Fraction parameter	[1]
	β	0.1	Scatter parameter	[2],[3]
	SCAT	True	Scatter parameter	[1]
	N_{PTRM}	2	Number of pTRM checks	
	n	4	number of data points	
	MAD	5	Maximum Angular Deviation of the zero field steps	[4]
	DANG	10	Deviation Angle	[5]
	alteration check (correction)	5%	Alteration check in Non-Linear-TRM, TRM anisotropy, and cooling rate experiments	
Sample paleointensity	N_{min}	3		
	$N_{min\_aniso\_corr}$	at least half of the specimens	Minimum number of specimens with anisotropy correction	
	$N_{min\_cr\_corr}$	1	Minimum number of specimens with cooling rate correction	
	σ	$\sigma < 3\ \mu T$ OR $\sigma\% < 8\%$	Standard deviation of the sample mean	
	anisotropy sample test	1%	If the mean anisotropy correction of all the specimens from the same sample is higher than 5% then specimens without anisotropy correction are discarded	
Specimen direction	MAD	5	Maximum Angular Deviation	[4]
Sample direction	N	8	minimum number of specimens for mean calculation	
	K	50	Fisher precision parameter	[6]

[a] For a complete description and definitions see Paterson et al. (2014) (http://www.paleomag.net/SPD/)
[b] [1]: Shaar and Tauxe (2013); [2]: Coe et al., (1978); [3]: Selkin and Tauxe (2000) [4]: Kirschvink (1980); [5] Tauxe and Staudigel (2004); [6] Fisher (1953)

Table 2: Paleointensity data (shown in Figures 3,5)

stratum	Age (BCE)	sample	Megiddo reference	n	B ± σ	VADM ± σ	B error envelope	VADM error envelope
H-03	740 (800-732)	mgh03b	94/H/067/VS 1	5	75.09±2.59	142.0±4.9	66.8-83.5	126.3-157.9
		mgh03f	94/H/008/VS 1	5	81.08±2.54	153.3±4.8	71.4-89.2	135.0-168.7
		mgh03g	96/H/060/VS 2	8	93.49±4.76	176.8±9.0	83.0-104.7	157.0-198.0
		mgh03h	94/H/075/VS 2	7	76.04±3.19	143.8±6.0	68.6-83.6	129.7-158.1
		mgh03i	98/H/006/VS 2	6	79.90±1.21	151.1±2.3	69.3-86.3	131.0-163.2
		mgh03j	96/H/005/VS 1	3	89.87±0.26	169.9±0.5	80.4-91.9	152.0-173.8
H-07	900 (950-850)	mgh07b	06/H/78 Vs 8	4	74.61±2.11	141.1±4.0	70.2-81.0	132.7-153.2
		mgh07d	06/H/26 Vs 4	5	67.84±2.41	128.3±4.6	59.3-77.5	112.1-146.6
Q-05	900 (950-850)	mgq05t1PI	Square C/5 L. 10/Q/126	3	68.65±0.69	129.8±1.3	62.4-81.2	118.0-153.5
		mgq05t2PI	Square G/5 L. 10/Q/131	6	64.14±1.27	121.3±2.4	61.3-72.4	115.9-136.9
H-09	1000 (1050-950)	mgh09h	08/H/35 Vs 3	5	66.54±0.30	125.8±0.6	65.3-69.8	123.5-132.0
		mgh09j	08/H/13 Vs 1	4	73.79±0.04	139.5±0.0	71.7-76.0	135.6-143.7
		mgh09k	06/H/55 Vs 11	5	82.89±0.14	156.7±0.2	71.5-86.0	135.2-162.6
		mgh09l	08/H/019/VS 4	4	79.33±0.42	150.0±0.8	75.2-88.5	142.2-167.4
		mgh09m	08/H/34 Vs 5	6	67.08±2.71	126.8±5.1	61.1-70.5	115.5-133.3
H-12	1125 (1150-1100)	mgh12t1PI		5	63.20±1.86	119.5±3.5	56.9-67.8	107.6-128.2
K-06	1130 (1130-1180)	mgk06a	04K/44 Vs 6	6	66.38±0.91	125.5±1.7	59.6-75.3	112.7-142.4
		mgk06b	04/K/19 Vs 3	3	62.34±2.99	117.9±5.6	55.2-69.1	104.4-130.7
		mgk06c	04/K/44 Vs 3	5	62.50±2.25	118.2±4.2	56.3-66.6	106.5-125.9
		mgk06d	04/K/42 Vs 2	5	59.87±0.89	113.2±1.7	53.9-64.2	101.9-121.4
K-08	1250 (1300-1200)	mgk08a	06/K/043/VS 6	5	59.60±1.02	112.7±1.9	57.4-65.8	108.5-124.4
		mgk08b	06/K/012/VS 5	5	58.26±3.51	110.2±6.6	52.9-64.4	100.0-121.8
		mgk08c	06/K/012/VS 7	4	62.86±0.27	118.9±0.5	56.8-67.6	107.4-127.8
		mgk08e	06/K/090/VS 5	5	55.60±0.83	105.1±1.6	51.0-60.4	96.4-114.2
K-09	1350 (1400-1300)	mgk09t1PI	Square P/10/11	3	52.35±3.99	99.0±7.5	48.0-56.3	90.8-106.5
F-10	1450 (1500-1400)	mgf10a	98/F/071/VS 2	4	49.81±0.52	94.2±1.0	46.9-53.3	88.7-100.8
		mgf10b	98/F/087/VS 1	5	50.01±2.78	94.6±5.2	46.1-54.4	87.2-102.9
		mgf10d	98/F/099/VS 3	4	52.07±2.31	98.5±4.4	47.3-57.4	89.4-108.5
F-13	1800 (1900-	mgf13b	00/F/123/VS 1	7	38.43±1.95	72.7±3.7	34.4-42.1	65.1-79.6
		mgf13d	00/F/123/VS 1	6	42.70±0.98	80.7±1.8	40.4-46.1	76.4-87.2

	1700)							
		mgf13e	00/F/092/VS 1	7	42.01±2.89	79.4±5.5	39.1-44.9	73.9-84.9
		mgf13f	00/F/092/VS 4	4	42.83±0.22	81.0±0.4	39.3-46.9	74.3-88.7
J-04	3000 (3100-2900)	mgj04a	98/J/021/VS 5	3	31.87±1.09	60.3±2.0	28.8-33.6	54.5-63.5
		mgj04b	98/J/021/VS 1	5	42.34±2.65	80.1±5.0	38.5-46.9	72.8-88.7
		mgj04d	96/J/056/VS 8	8	35.27±2.29	66.7±4.3	31.7-39.0	59.9-73.7
J-06	2750 (2700-2800)	mgj06a	04/J/072/VS 2	4	38.42±2.97	72.7±5.6	35.4-41.7	66.9-78.9
		mgj06b	04/J/050/VS 2	3	39.25±0.10	74.2±0.2	35.0-42.3	66.2-80.0
		mgj06c	04/J/072/VS 1	4	40.41±1.26	76.4±2.4	37.8-46.3	71.5-87.6
		mgj06d	04/J/096/VS 1	3	37.02±0.07	70.0±0.1	35.7-40.9	67.5-77.3